

## Design and implementation of AMD system for response control in tall buildings

J. Teng\*, H.B. Xing, Y.Q. Xiao, C.Y. Liu, H. Li and J.P. Ou

*Harbin Institute of Technology Shenzhen Graduate School, Shenzhen, China*

*(Received June 15, 2012, Revised June 17, 2013, Accepted October 29, 2013)*

**Abstract.** This paper mainly introduces recently developed technologies pertaining to the design and implementation of Active Mass Damper (AMD) control system on a high-rise building subjected to wind load. Discussions include introduction of real structure and the control system, the establishment of analytical model, the design and optimization of a variety of controllers, the design of time-varying variable gain feedback control strategy for limiting auxiliary mass stroke, and the design and optimization of AMD control devices. The results presented in this paper demonstrate that the proposed AMD control systems can resolve the issues pertaining to insufficient floor stiffness of the building. The control system operates well and has a good sensitivity.

**Keywords:** Active Mass Damper; variable gain feedback control; limiting auxiliary mass stroke; optimization

---

### 1. Introduction

Since the introduction of control concepts for response mitigation in civil engineering structures (Yao 1972), active control in civil engineering has advanced from theoretical analysis and experimental research to engineering application. Active control devices have been used in several structures in variety of forms (Satoru *et al.* 1988, Akira 1998, Cao *et al.* 1998, Akira *et al.* 2001, Masashi *et al.* 2001, Yoshiki *et al.* 2001, Ji Chunyan *et al.* 2004, Yoshiki 2009). Aizawa *et al.* (1988) developed a four layers framework model vibration table experiment by setting an AMD control system. The Kyobashi Center building in Tokyo, Japan (Yoshiki *et al.* 2001) was the first structure installed with an AMD control system in the world. Osaka, Kanazawa, and other Japanese cities have also built many sets of AMD control system (Yoshiki 2009). T.T. Soong (Cao *et al.* 1998) implemented an AMD control system in the Nanjing TV Tower for controlling wind vibration. AMDs have great potential as a vibration control device, however the number of structures with AMDs are less than other control devices (Yoshiki 2009). This is due to the issues pertaining to implementation, such as the controller design and operation of AMD.

Many researchers have worked on addressing these issues. Yushida *et al.* (1986) have built controllers with no-conditional feedback gains by selecting the best gain that will result in optimal driving force. Several other researchers (Fujita *et al.* 1992, Suzuki *et al.* 1993, Kawai *et al.* 1994)

---

\*Corresponding author, Professor, E-mail: [tengj@hit.edu.cn](mailto:tengj@hit.edu.cn)

used the same method to establish discrete control gains dependent on AMD-displacement and velocity. Based on Linear Quadratic Regulator (LQR) control algorithm and the degree of the external excitations, Ichiro Nagashima and Yuzo Shinozaki (1997) selected the specified best weight matrix to get the corresponding feedback gain and thus to realize auxiliary mass stroke optimal control.

This paper briefly introduces the technologies and methodologies used in the design and implementation of an AMD control system for a high-rise building in Shenzhen, China.

## 2. Objective building and AMD system

Fig.1 shows the high-rise building and AMD control system.

The building has a height of  $441.8m$  with 102 floors, in which 98 floors are above the ground, and 4 layers are underground. The structure has an AMD system in the 91<sup>st</sup> floor. The ratio of structural height to width is 10.2, and that of the core-tube is 19.1. The building used the steel framework and concrete core-tube structure system with giant steel braces, arms outstretched truss and waist truss to improve its lateral stiffness. The out surface structure used steel tube concrete columns, steel beams and steel braces, while the core-tube used steel concrete.

The control system includes two sets of synchronous AMD devices (servo motor driving control system), shown in Fig. 1(b). The devices are located on both sides of the 91<sup>st</sup> floor, mainly used to control wind-induced vibration along weak axial ( $Y$  direction) of the structure. The specific parameters of the AMD control system are shown in Table 1. It should be noted that there are two sets of synchronous AMD devices, so some parameters in Table 1 should be multiplied by 2.

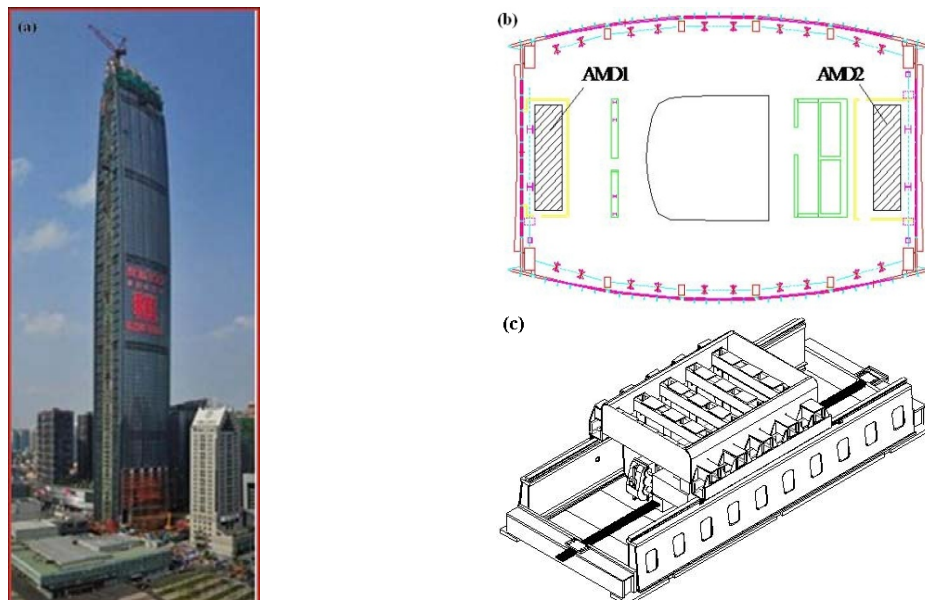


Fig. 1 Objective building and AMD systems: (a) Objective building, (b) locations of AMD systems and (c) an AMD system

Table 1 The Parameters of AMD Control System

Index	AMD
Auxiliary mass ( $t$ )	250×2
Effective stroke ( $m$ )	±2.2
Maximum driving force ( $kN$ )	275×2
Peak power ( $kW$ )	300×2

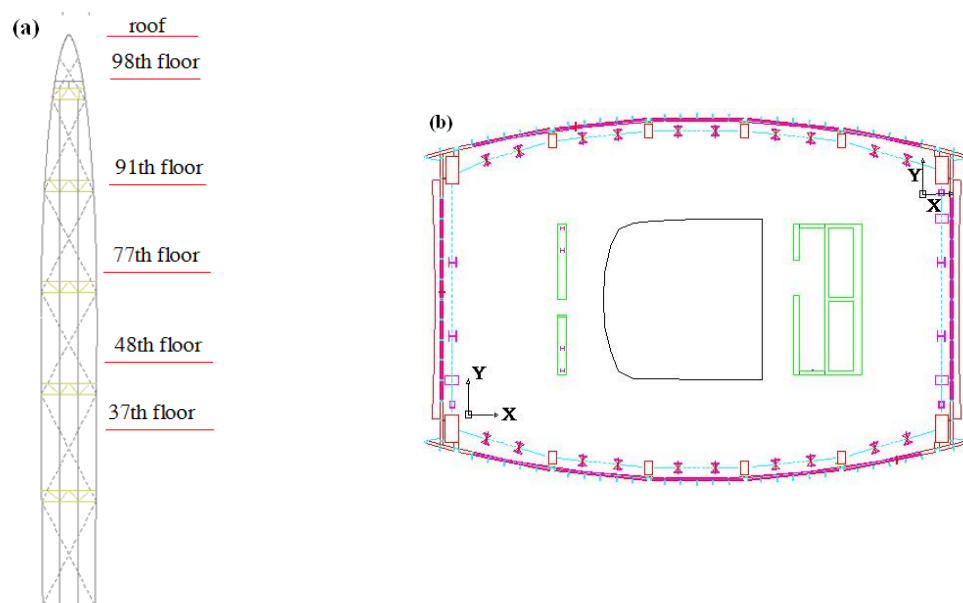


Fig. 2 Acceleration sensors arrangement: (a) Vertical arrangement, (b) Level arrangement

The AMD control system installed in the building uses the state feedback strategy. The states are estimated from the floor accelerations measured by accelerometers in the structure. Accelerometers are installed in the 37<sup>th</sup>, 48<sup>th</sup>, 77<sup>th</sup>, 91<sup>st</sup>, 98<sup>th</sup> floors and the roof of structure. Each floor has 4 accelerometers, as shown in Fig. 2(b). They are located in the floor plane diagonally to measure the acceleration of  $X$  and  $Y$  direction.  $Y$ -direction acceleration is used to identify the feedback state and comfortable performance of the structure, whereas  $X$ -direction acceleration is used to identify structural comfortable performance only.

### 3. Simplified model and verification

Since the original structure has many degrees of freedom (DOFs), the online computation cannot satisfy the requirements of real time control. So, the order of the original structure needs to be reduced.

### 3.1 Establishment of simplified model

To retain the original structure dynamic behavior along weak axis ( $Y$  direction), a new model is created. The following procedure is used for model reduction: (1) Centralizing the mass of each floor in the original structure in order to form the vertical mass unit series model. (2) Based on the vertical sizes and the changing stiffness, several adjacent mass units are condensed to one mass unit and thus forming a simplified model with 24 mass unit series in the vertical direction. The mass matrix of the simplified model is a diagonal matrix with 24 elements. (3) Unit-displacement method is used to calculate the flexibility matrix. Unit horizontal load is applied at a mass point of condensed element model and displacements at all other locations are calculated. This will make one column of the flexibility matrix of the simplified model. Assembling all the columns the flexibility matrix is obtained, and then by inverting the flexibility matrix we can get the stiffness matrix. Since the FE model is based on the original structure, thus the stiffness matrix here has taken into account of the structural flexural deformation and shear deformation.

### 3.2 Verification of simplified model

To verify the accuracy of the simplified model, the structural periods of first six vibration modes calculated from this simplified model are compared with the full finite element model. The results show that the simplified model can capture the dynamic behavior of the actual structure well. The full finite element model will be referred as FE model from here on.

To further verify the simplified model, dynamic responses of the simplified model and the FE model under the same fluctuating wind loads (e.g., ten-years return fluctuating wind) on the key floor, for instance the 87<sup>th</sup>, are investigated and compared. Results indicate that the two models have a good agreement. The maximum error of the structural peak displacement is only 0.37% and that of the top floor peak displacement is less than 0.3%. Relatively, the errors in peak accelerations are larger than those of peak displacements. The error of peak acceleration on the top floor (98th floor) is 5.34%. This is due to two reasons: (1) Structural acceleration is severely affected by the higher order vibration modes and hence it requires more accurate simplified model to capture acceleration than displacement. (2) The influence of the top roof truss in actual building structure.

## 4. Control strategies

AMD control system (that is, Active Mass damper or Driver control system) is a system which can mitigate the dynamic response of the structure by applying optimal control force computed based on the control strategy and feedback signals to the controlled structure. The state equation for an AMD control system is

$$\begin{cases} \dot{Z}(t) = AZ(t) + Bu(t) \\ Y(t) = CZ(t) + Du(t) \end{cases} \quad (1)$$

where,  $A$ ,  $B$ ,  $C$ ,  $D$  is the state matrix, input matrix, output matrix and feed-forward matrix, respectively.  $Z(t)$  is the state vector and  $u(t)$  is the control force.

In this paper, the LQR control algorithm, Pole Assignment (PA) control algorithm, and Fuzzy

Neural Network (FNN) control algorithm were evaluated for the simplified model and AMD assembly. Additionally, performances of AMD control system under auxiliary mass of 400 tons, 500 tons, and 600 tons are also studied.

#### 4.1 LQR control algorithm

For the AMD control system shown as equation (1), the control force,  $u(t)$ , can be got by LQR control algorithm is (Soong *et al.* 1994)

$$u(t) = -R^{-1}(t)B^T P(t)Z(t) \tag{2}$$

where,  $P(t)$  is calculated from the following Riccati equation

$$\dot{P}(t) = -P(t)A + P(t)BR^{-1}(t)B^T P(t) - A^T P(t) - Q(t) \tag{3}$$

where,  $Q(t), R(t)$  are weight-matrices and their values are selected depending on the relative importance given to the different terms in their contribution to the performance index.

Based on the building specific functions, an improvement is made to the ordinary LQR control algorithm, by setting the weight coefficients corresponding to the 87<sup>th</sup> floor displacement and auxiliary mass displacement to  $1.9 \times 10^5$  and  $0.7 \times 10^3$  in weight matrix  $Q$  (others being 0), and the weight coefficient corresponding to the control force in  $R$  to  $1.0 \times 10^{-3}$ . Using this modified control algorithm, the uncontrolled and controlled structural responses, driving forces, and strokes are summarized in Table 2.

Table2 Comparison of the structural responses under ten years appeared fluctuating wind

Index		Uncontrolled	LQR controlled		
			600	500	400
87 <sup>th</sup> floor	Auxiliary mass (T)				
	Displacement peak value (m)	0.25	0.18	0.19	0.20
	Accelerate peak value (gal)	20.80	15.54	16.00	16.33
	Displacement mean-square deviation (m)	0.08	0.05	0.06	0.06
	Accelerate mean-square deviation (gal)	6.40	4.66	4.90	5.05
92 <sup>th</sup> floor	Displacement peak value (m)	0.26	0.20	0.21	0.21
	Accelerate peak value (gal)	23.30	18.41	18.88	19.17
	Displacement mean-square deviation (m)	0.08	0.06	0.06	0.06
	Accelerate mean-square deviation (gal)	7.10	5.37	5.60	5.75
98 <sup>th</sup> floor	Displacement peak value (m)	0.28	0.21	0.23	0.23
	Accelerate peak value (gal)	37.40	30.01	31.49	31.99
	Displacement mean-square deviation (m)	0.09	0.06	0.07	0.07
	Accelerate mean-square deviation (gal)	9.50	8.03	8.21	8.33
	Stroke ( $m$ )	—	1.96	1.86	1.98
	Driving force ( $kN$ )	—	600	550	550

note : Driving force in chart is a limit value under the consideration of realistic driving system work power

From Table 2, it can be confirmed that the AMD control system can decrease the structural dynamic response significantly. For example, with an auxiliary mass of 500 tons, the peak acceleration of 87<sup>th</sup> floor decreased from 20.80gal to 16.00gal with the addition of AMD. The reduction with the addition of AMD is 21.40%, and that of floor displacement peak value is 18.17%. In addition, the 87<sup>th</sup> floor control effect is superior to that of upper floors. This is due to the optimization to the weight matrix of 87<sup>th</sup> floor. From Table 2, it is clear that increasing the mass of AMD will improve the performance of the closed loop system.

Fig.3 shows the envelope curve of structural dynamic responses' peak value and mean value under ten-year return period wind load.

The AMD control system with LQR control algorithm has a better control effect on the upper floors' displacements than that of the lower floors' displacements. The reductions in acceleration of the floor in which the AMD is installed and the adjacent floors is better than those of other floors.

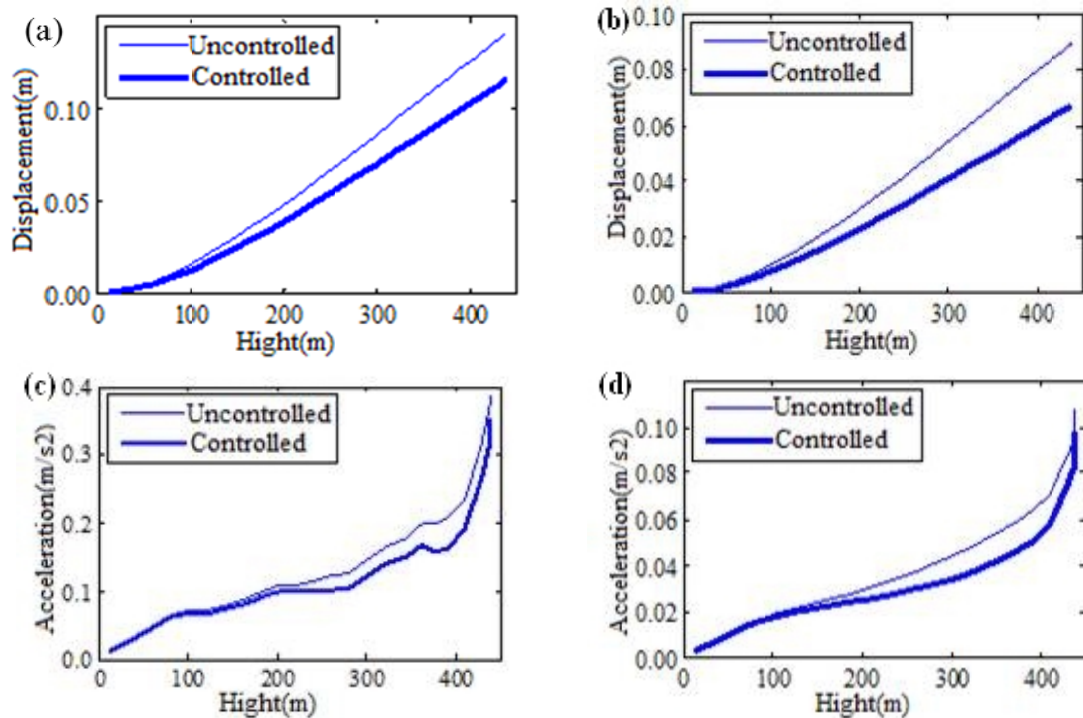


Fig. 3 Comparison of structural responses under controlled and uncontrolled conditions: (a) Comparison of peak displacement, (b) Comparison of mean square displacement, (c) Comparison of peak acceleration, (d) Comparison of mean square acceleration .). Comparison of structural responses under controlled and uncontrolled conditions: (a) Comparison of peak displacement, (b) Comparison of mean square displacement, (c) Comparison of peak acceleration, (d) Comparison of mean square acceleration

#### 4.2 Pole assignment control algorithm

Since the sum of the modal participating factors of first three structural vibration modes is 79.80%, the desired closed loop performance is guaranteed by placing the poles based on the first three vibration modes. The control force of the AMD system as per the PA control algorithm is (Ou 2003)

$$u(t) = \{e\}[\Gamma]^{-1} Z(t) \quad (4)$$

where,  $[\Gamma]$  is a matrix composed by the linear independence column vector in the characteristic vector matrix;  $\{e\}$  is the linear independence column position matrix. Based on Eq. (4), the controlled and uncontrolled structural dynamic response, and the AMD control system performance index are summarized in Table 3.

Comparison the response reductions in Tables 3 and 2, it is clear that the performance of PA control system is superior compared to that of LQR control system, specifically in acceleration.

Table 3 Comparison of the structural responses under ten years appeared fluctuating wind

Index		Uncontrolled	Pole Assignment control		
			600	500	400
87 <sup>th</sup> floor	Auxiliary mass (T)				
	Displacement peak value (m)	0.25	0.18	0.19	0.20
	Acceleration peak value (gal)	20.80	14.25	15.10	15.58
	Displacement mean-square deviation (m)	0.08	0.05	0.06	0.06
	Acceleration mean-square deviation (gal)	6.40	4.32	4.62	4.76
92 <sup>th</sup> floor	Displacement peak value (m)	0.26	0.20	0.20	0.21
	Acceleration peak value (gal)	23.30	16.60	17.68	18.20
	Displacement mean-square deviation (m)	0.08	0.06	0.06	0.06
	Acceleration mean-square deviation (gal)	7.10	4.73	5.03	5.27
98 <sup>th</sup> floor	Displacement peak value (m)	0.28	0.21	0.22	0.23
	Acceleration peak value (gal)	37.40	28.33	30.53	29.59
	Displacement mean-square deviation (m)	0.09	0.06	0.06	0.07
	Acceleration mean-square deviation (gal)	9.50	6.90	7.78	7.56
	Stroke(m)	—	1.93	1.99	1.96
	Driving force (k N)	—	600	550	550

note : Driving force in chart is a limit value under the consideration of realistic driving system work power.

This is due to the fact that the LQR control system weight matrices are optimized to control system states (displacement and velocity) and control force, but not acceleration. While PA algorithm is effective in reducing the structure response including acceleration since it is based on the poles which affect the entire structural dynamic response. It shows that, compared to LQR algorithm, PA algorithm is more suitable for improving structural comfort under wind-induced vibration.

To further illustrate this point, we give an example of analyzing the structural damping ratios (auxiliary mass 500 tons) using the uncontrolled structure, LQR algorithm controlled structure and PA algorithm controlled structure respectively. The results are shown in Table 4 below.

Table 4 The first four damping ratio

Control algorithm	First mode damping	Second mode damping	Third mode damping	Forth mode damping
Uncontrolled structure	0.015	0.015	0.015	0.015
LQR controlled	0.031	0.017	0.016	0.016
Pole Assignment controlled	0.032	0.032	0.027	0.015

The results in Table 4 indicate that both the control systems can increase effective damping of closed loop system. The amount of increase in structural damping using PA is better than that of LQR control system. This further justify that PA is more suitable for controlling structural wind-induced vibration. The result is consistent with the above theoretical analysis.

#### 4.3 Fuzzy neural network control algorithm

Based on the preliminary FNN theory of Takagi-Sugeno model, a FNN predictive model is established for the high-rise building and also a FNN predictive controller (assuming floor acceleration as input parameter) using clustering method (Ou J.P. 2003). The control force is

$$U(k+1) = f(a_{65}(k), a_{87}(k), a_{98}(k), U(k); W) \quad (5)$$

where  $a_{65}(k)$ ,  $a_{87}(k)$ ,  $a_{98}(k)$  are accelerations of the 65<sup>th</sup> floor, 87<sup>th</sup> floor, and 98<sup>th</sup> floor, respectively for time step- $k$ .  $U(k)$  is the control force at moment  $k$  and  $W$  is a weight matrix. The summary of dynamic response using AMD and FNN predictive controller are shown in the Table 5.

Table 5 demonstrates that the FNN control system is capable of reducing structural dynamic response. For AMD with 500 tons auxiliary mass, the 87<sup>th</sup> floor's acceleration peak value has decreased from 20.80gal to 15.05gal. The control effect is 27.67%. The displacement peak value has also decreased from 0.25 m to 0.17 m. The control effect is 31.54%. In addition, the control

effect of acceleration mean-square deviation and displacement mean-square deviation are both more than 30%. From Table 5, it is also clear that FNN algorithm has a better control effect of structural displacement peak value than that of displacement mean-square deviation.

Table 5 Comparison of the structural responses under ten years appeared fluctuating wind

Index		Uncontrolled	FNN control		
Auxiliary mass ( $T$ )			600	500	400
87 <sup>th</sup> floor	Displacement peak value (m)	0.25	0.17	0.17	0.17
	Acceleration peak value (gal)	20.80	14.70	15.05	15.50
	Displacement mean-square deviation (m)	0.08	0.05	0.05	0.06
	Acceleration mean-square deviation (gal)	6.40	4.34	4.48	4.60
92 <sup>th</sup> floor	Displacement peak value (m)	0.26	0.18	0.18	0.18
	Acceleration peak value (gal)	23.30	17.10	17.59	18.14
	Displacement mean-square deviation (m)	0.08	0.05	0.05	0.06
	Acceleration mean-square deviation (gal)	7.10	4.99	5.03	5.29
98 <sup>th</sup> floor	Displacement peak value (m)	0.28	0.19	0.19	0.19
	Acceleration peak value (gal)	37.40	29.68	29.80	30.10
	Displacement mean-square deviation (m)	0.09	0.06	0.06	0.07
	Acceleration mean-square deviation (gal)	9.50	7.62	7.73	7.80
Stroke( $m$ )		—	1.96	1.93	1.93
Driving force ( $kN$ )		—	600	600	600

note : Driving force in chart is a limit value under the consideration of realistic driving system work power.

#### 4.4 Selection of control strategy

From above analyses, all the three control algorithms have similar effects on controlling structural dynamic responses under the external excitations. Considering acceleration control, the response of all the three algorithms are summarized in Table 6.

From Table 6, it is clear that the control effects of the acceleration of the three algorithms are all more than 20%. PA and FNN control algorithms have similar control effects, and they have superior performance compared to LQR algorithm. PA is stable and is widely used. However, its calculation model requires high accuracy. FNN control algorithm requires a less number of sensors, but its rule library is associated with the stochastic wind load.

As a result, in this paper we choose PA as the control algorithm for our system. Meanwhile, the FNN control algorithm was used as an alternative to verify PA control algorithm. Considering the actual structural conditions, the auxiliary mass of AMD is determined as 500 tons, which is equivalent to 0.47% total mass of structure in its first vibration mode.

Table 6 Comparison of control effect (%)

Auxiliary mass ( $T$ )	Acceleration	LQR control	PA control	FNN control	Force (kN)	Stroke (m)	Difficulty
400	Peak value	21.48	25.08	25.48	550	1.980	Simple to realize
	Mean-square deviation	21.14	25.69	28.13			
500	Peak value	23.10	27.40	27.67	550	1.900	Simple to realize
	Mean-square deviation	23.48	27.88	30.02			
600	Peak value	25.28	31.48	29.35	600	1.977	Simple to realize
	Mean-square deviation	27.13	32.54	32.13			

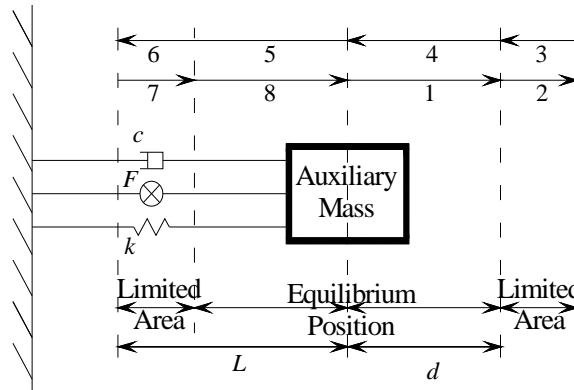


Fig. 4 A sketch of an AMD control system

## 5. Limitation of AMD displacement (stroke)

### 5.1 Limitation principle

Auxiliary mass operation in AMD control systems is shown in Fig. 4.  $d$  is defined as the Threshold Limit Value which shows operation length of the auxiliary mass.  $L$  is the maximum allowable relative displacement (namely the stroke) which is less than entire rail length and more than that of  $d$ .  $k$ ,  $c$  and  $F$  denotes the stiffness, damping and driving force of the AMD control system, respectively. No.1 to No.8 in Fig. 4 represent eight running states with arrows indicating the operation direction.

The auxiliary mass enters the limited area when AMD system location is out of  $d$ . In this condition it may collide with anti-collision device, produce noise, and pose a threat to both the AMD control system and structural safety if it has excessive velocity. So the additional objective of the control algorithm should be to set the relative displacement and relative velocity of auxiliary mass as controlling goals.

When auxiliary mass moves from limited area to the equilibrium position (operation state 3 and 7), the relative displacement and relative velocity of auxiliary mass are easy to overshoot which is

insignificant. Therefore, this paper only discusses the auxiliary mass's relative displacement and relative velocity control when the auxiliary mass is in the limited area and away from the equilibrium position (Operating state 2 and 6). Define the 2 and 6 operating states as limited states at which the relative displacement and relative velocity of auxiliary mass are in the same direction. The relative displacement and relative velocity of the auxiliary mass in this paper are referred to the displacement and velocity of the floor where the auxiliary mass locates.

### 5.2 Analysis of the principle

For a structural system composed of  $n$  mass points and one AMD control system shown as Eq. (1), the system state vector  $Z$  is

$$\begin{aligned} Z &= \{z_1 \quad z_2 \quad \dots \quad z_{2n+2}\}^T \\ &= \{y_1 \quad \dots \quad y_l \quad \dots \quad y_{n+1} \quad \dot{y}_1 \quad \dot{y}_2 \quad \dots \quad \dot{y}_n \quad \dot{y}_{n+1}\}^T \end{aligned} \quad (6)$$

where,  $y_i, \dot{y}_i, y_{n+1}, \dot{y}_{n+1}$  are the absolute displacement, velocity of  $i^{\text{th}}$  floor and AMD's absolute displacement and velocity respectively. Assuming that the number of floor where AMD control system is installed is  $l$ , the relative displacement and relative velocity of the auxiliary mass are  $z_{n+1} - z_l, z_{2n+2} - z_{l+n+1}$  respectively. These are the two goals discussed above.

The structural state  $z_i$  can't be directly controlled by the AMD control system, whereas the driving force  $F(t)$  can be controlled arbitrarily by adjusting feedback gain. At the same time, the driving force has direct relationship with the state vector and feedback gain. If we setup an equation between state vectors and feedback gains through the driving force, then we can control the state vectors or relative displacement and relative velocity of the auxiliary mass.

The driving force of system is

$$F(t) = -G(t) \cdot Z(t) = -\sum_{i=1}^{2n+2} g_i(t) z_i(t) = \sum_{i=1}^{2n+2} u_i(t) \quad (7)$$

where  $u_i(t)$  is the  $i^{\text{th}}$  component state vector contributing to driving force.  $G$  is feedback gain of the system.

$$G = \{g_1 \quad \dots \quad g_l \quad \dots \quad g_{n+1} \quad \dots \quad g_{2n+2}\} \quad (8)$$

where  $g_l$  and  $g_{n+1}$  are the gains according to displacement of the floor where AMD is installed and auxiliary mass respectively.

Since the general civil engineering structures (or simplified model) have a lot of DOFs and system state feedback gains, calculating all the states in real time will be time consuming. So the driving force is set as

$$F^*(t) = -[g_l(t)z_l(t) + g_{n+1}(t)z_{n+1}(t)] \quad (9)$$

if,  $u_i = 0, i \neq l, n+1$ , and  $g_l(t) = -g_{n+1}(t)$ , then

$$F^*(t) = -g_{n+1}(t)[z_{n+1}(t) - z_l(t)] = -g_{n+1}(t)x(t) \quad (10)$$

So

$$g_{n+1}(t) = -F^*(t)/x(t) \tag{11}$$

where  $x(t) > d > 0$ , is the stroke of auxiliary mass.

From Eq. (11), it is clear that the driving force has opposite sign of  $x(t)$  if  $g_{n+1}(t) > 0$ . Otherwise driving force and  $x(t)$  are in the same direction. According to the limitation principle, when auxiliary mass is located at the limitation state, driving force must be reverse to relative displacement  $x(t)$ , so  $g_{n+1}(t) > 0$ . Since relative displacement and relative velocity of auxiliary mass are in the same direction, the relative velocity is limited while we limit the relative displacement of auxiliary mass.

Once the driving force  $F^*(t)$  is known, the feedback gain  $g_{n+1}(t)$  can be calculated using Eq. (11). The feedback gain vector at limitation state is

$$G = \{0 \quad \dots \quad -g_{n+1}(t) \quad \dots \quad 0 \quad \dots \quad g_{n+1}(t) \quad \dots \quad 0\} \tag{12}$$

The feedback gain vectors at other states are invariant.

In a controlled limited displacement, relative velocity of auxiliary mass has a decreasing sinusoidal relationship with its relative displacement as showed in Fig. 5.

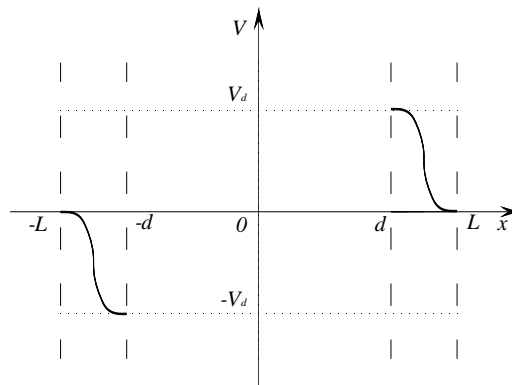


Fig. 5 A curve of the relationship between the relative velocity and relative displacement

Namely

$$V(x) = \begin{cases} \frac{1}{2}V_d \sin\left[\left(\frac{x-d}{L-d} + \frac{1}{2}\right) \cdot \pi\right] + \frac{1}{2}V_d & d \leq x \leq L \\ \frac{1}{2}V_d \sin\left[\left(\frac{-x-d}{L-d} - \frac{1}{2}\right) \cdot \pi\right] - \frac{1}{2}V_d & -L \leq x \leq -d \end{cases} \tag{13}$$

where ,  $V_d$ ,  $d$  and  $L$  are defined as above. The relative acceleration of auxiliary mass can be obtained by differentiating  $V(x)$ .

$$a(t) = \frac{dV}{dt} = \frac{dV}{dx} \cdot \frac{dx}{dt} = \begin{cases} \frac{\pi \cdot V_d}{2(L-d)} \left[ \cos\left(\frac{x-d}{L-d} + \frac{1}{2}\right)\pi \right] \cdot \dot{x} & d \leq x \leq L \\ \frac{-\pi \cdot V_d}{2(L-d)} \left[ \cos\left(\frac{-x-d}{L-d} - \frac{1}{2}\right)\pi \right] \cdot \dot{x} & -L \leq x \leq -d \end{cases} \quad (14)$$

Namely

$$a(t) = \begin{cases} \frac{\pi \cdot V_d^2}{4(L-d)} \left[ \cos\left(\frac{x-d}{L-d} + \frac{1}{2}\right)\pi \right] \cdot \left[ \sin\left(\frac{x-d}{L-d} + \frac{1}{2}\right)\pi + 1 \right] & d \leq x \leq L \\ \frac{\pi \cdot V_d^2}{4(L-d)} \left[ \cos\left(\frac{-x-d}{L-d} - \frac{1}{2}\right)\pi \right] \cdot \left[ \sin\left(\frac{x+d}{L-d} + \frac{1}{2}\right)\pi + 1 \right] & -L \leq x \leq -d \end{cases} \quad (15)$$

The driving force is

$$F^*(t) = M \cdot a(t) = \begin{cases} \frac{\pi \cdot M \cdot V_d^2}{4(L-d)} \left[ \cos\left(\frac{x-d}{L-d} + \frac{1}{2}\right)\pi \right] \cdot \left[ \sin\left(\frac{x-d}{L-d} + \frac{1}{2}\right)\pi + 1 \right] & d \leq |x| \leq L \\ \frac{\pi \cdot M \cdot V_d^2}{4(L-d)} \left[ \cos\left(\frac{-x-d}{L-d} - \frac{1}{2}\right)\pi \right] \cdot \left[ \sin\left(\frac{x+d}{L-d} + \frac{1}{2}\right)\pi + 1 \right] & -L \leq x \leq -d \end{cases} \quad (16)$$

The relationship curve between the driving force and relative displacement is shown in Fig. 6. The value of  $F_0$  is

$$F_0 = \left| \frac{\pi M V_d^2}{4(d-L)} \right| \quad (17)$$

Hence, we can get feedback gain through Eqs. (11) and (16).

$$g_{n+1}(t) = \begin{cases} \frac{\pi \cdot M \cdot V_d^2}{4(L-d)} \left[ \cos\left(\frac{x-d}{L-d} + \frac{1}{2}\right)\pi \right] \cdot \left[ \sin\left(\frac{x-d}{L-d} + \frac{1}{2}\right)\pi + 1 \right] / x(t) & d \leq x \leq L \\ \frac{\pi \cdot M \cdot V_d^2}{4(L-d)} \left[ \cos\left(\frac{-x-d}{L-d} - \frac{1}{2}\right)\pi \right] \cdot \left[ \sin\left(\frac{x+d}{L-d} + \frac{1}{2}\right)\pi + 1 \right] / x(t) & -L \leq x \leq -d \end{cases} \quad (18)$$

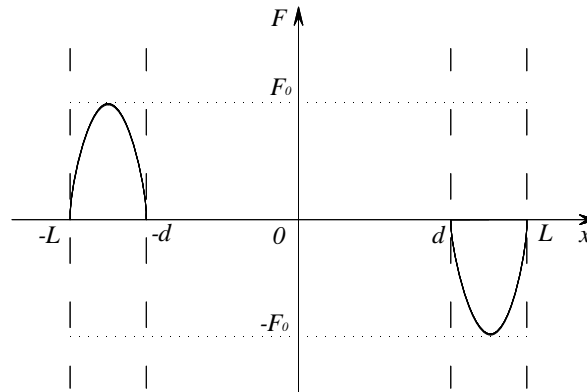


Fig. 6 A curve of the relationship between the driving force and displacement

### 5.3 Numerical simulation

The feedback gain for control system using Eq. (18) in which the only parameter to be determined is the Threshold Limit Value  $d$ . In this paper, we investigate the control effect of acceleration mean-square value on key floor (such as 87<sup>th</sup>), amplitude of the auxiliary mass's relative displacement and control force when  $d$  changes from 0 to  $L$  (2.1 m) with an interval of 0.1 m. The corresponding curves are shown in Figs. 7- 9.

Fig. 7 shows that the amplitude of the auxiliary mass' relative displacement decrease first and then increase with increasing  $d$ . Whereas control effects of acceleration mean-square value of 87<sup>th</sup> floor and the amplitude of driving force almost keep increasing in Figs. 8 and 9. That is because as the length of limit displacement becomes smaller, the velocity reduction duration time is getting shorter and the driving force becomes larger with increasing  $d$ . Meanwhile, as the auxiliary mass operates freely, the effect of the control system is better. System is stable with respect to the variation range of the control performance index.

From above analysis, the Threshold Limit Value  $d$  is 1.1 m. A comparison of the structural responses and system performance index between the Original System (OS) and the System with Control Limitation (SWCL) is shown in Fig. 10 to Fig. 12. Table 10 shows the control effects of the displacement and acceleration mean-square values on floor 87<sup>th</sup> with and without limited stroke, respectively.

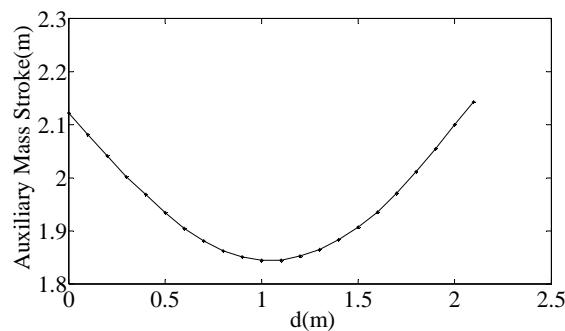


Fig. 7 A curve of the auxiliary mass stroke

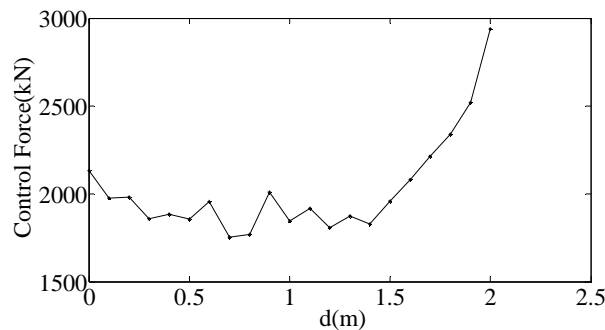


Fig. 8 A curve of thrust amplitudes

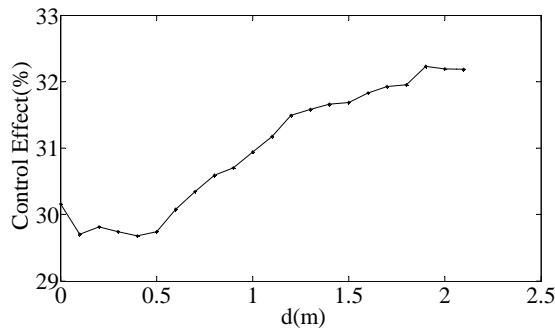


Fig. 9 A curve of the mean square values of control effect

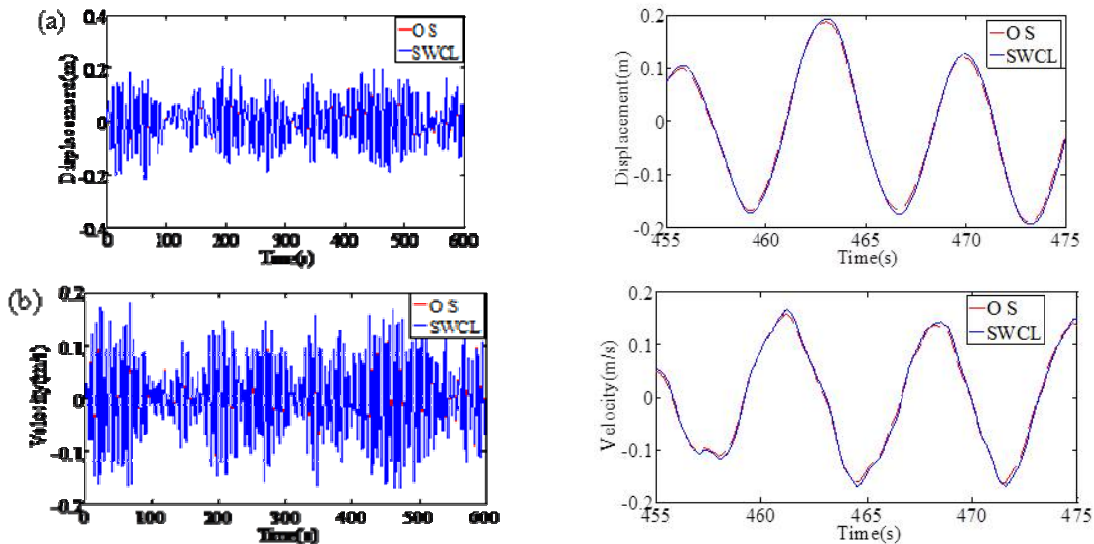


Fig. 10 A comparison of structural responses: (a) A comparison between displacements and (b) A comparison between velocities

From Fig. 10 to Fig. 12 it can be seen that when the relative displacement and relative velocity are limited, the dynamic responses (acceleration and displacement of 87<sup>th</sup> floor) will slightly increase. The control effect drops slightly but its amplitude is small, which is consistent with Table 10. When the relative displacement of auxiliary mass exceeds  $d$ , there is a sharp down curve in relative velocity and relative displacement. Its relative displacement will not be smaller than  $d$  while its relative velocity will nearly become zero at the same time. This indicates that current control algorithm can realize controlling relative velocity and relative displacement (or stroke) simultaneously. Meanwhile, the system power consumption significantly increases, because the relative velocity of auxiliary mass changes largely after it enters the limitation area. In practice, antilock braking force can be used to replace the driving force to limit auxiliary mass stroke and relative velocity.

In brief, the control algorithm designed in this paper can well limit the auxiliary mass's relative displacement (or stroke) and relative velocity in order to ensure the security of the control system and the structure. The control system does not change the system performance yet.

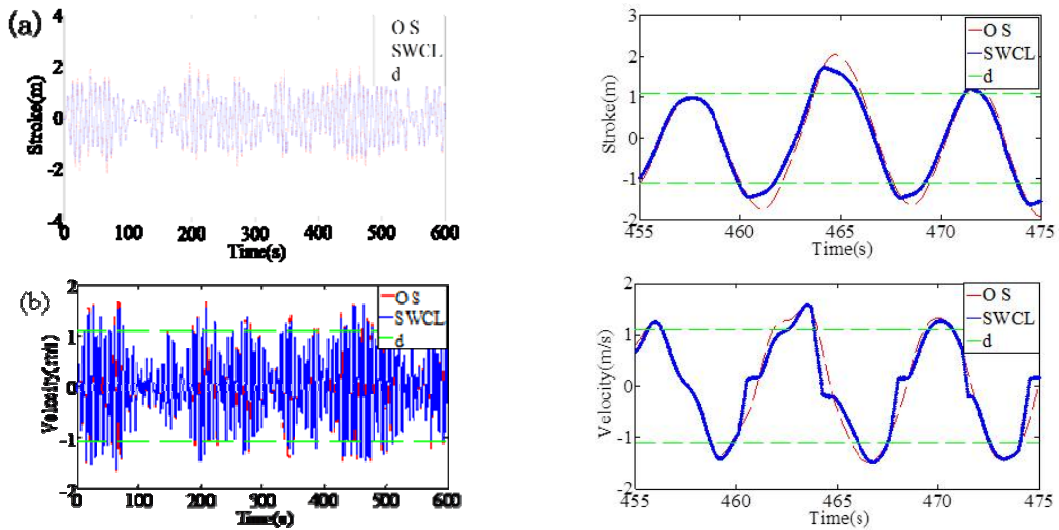


Fig. 11 A comparison of AMD parameters: (a) A comparison of auxiliary mass strokes and (b) A comparison of auxiliary mass velocities

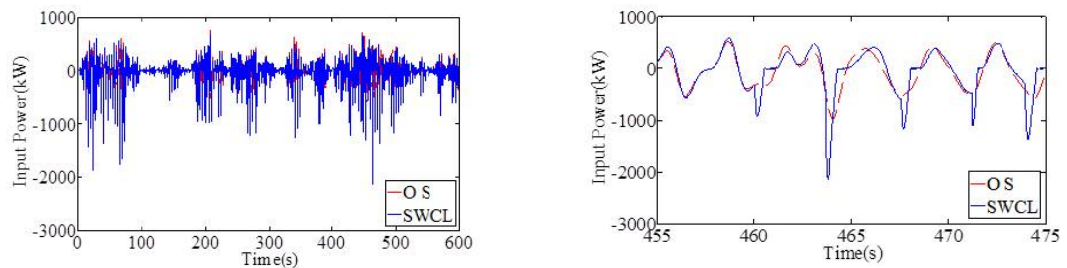


Fig. 12 A comparison of the input power

Table10 A comparison of mean-square values of control effect under limited stroke

Floor	Displacement		Acceleration	
	Without limitation	Limitation	Without limitation	Limitation
87th	30.95%	29.99%	32.35%	30.69%
92nd	30.99%	30.02%	31.42%	27.76%
98th	31.02%	30.04%	26.42%	25.08%

## 6. AMD control devices

### 6.1 The components of the control device

The AMD control device is shown in Fig. 1. It is mainly composed of girder base, servo motor, guideway, gear-rack and hydraulic floating installation. The components are shown in Fig. 13.

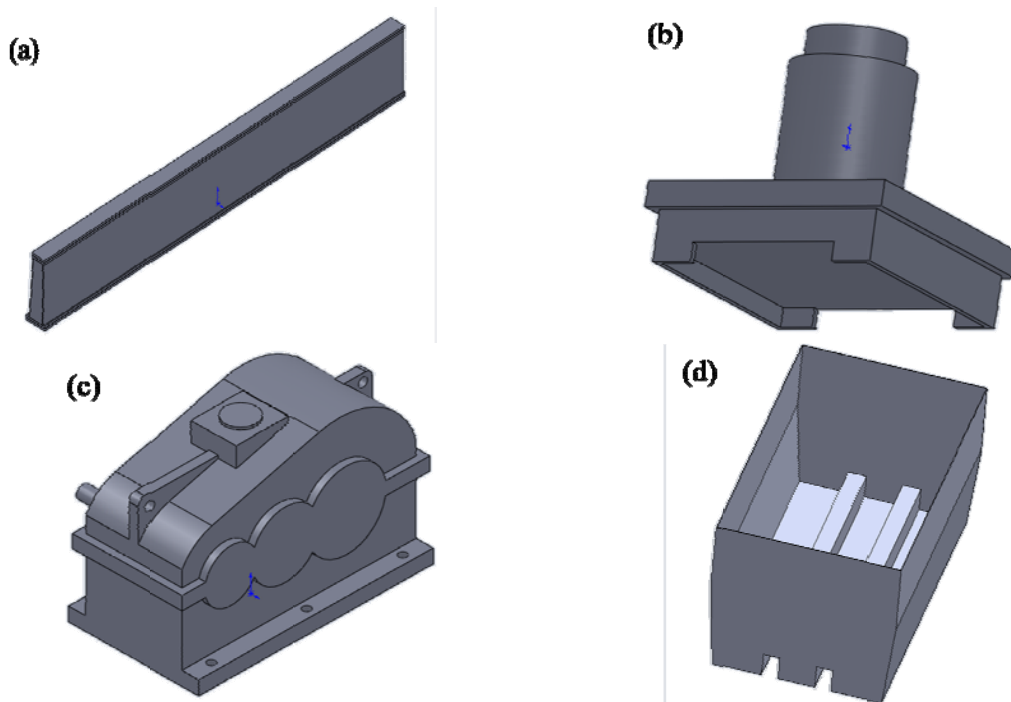


Fig. 13 the components of the AMD control devices: (a) Girder base, (b) Hydraulic floating installation, (c) Reducer and (d) Loading bucket

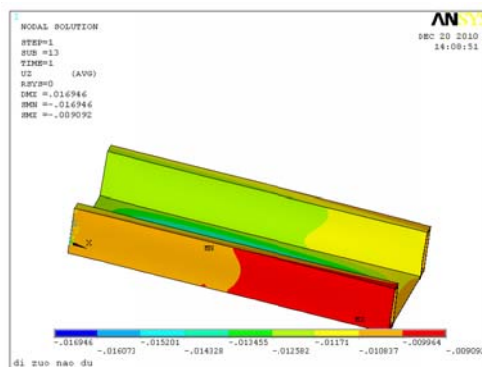


Fig. 14 the cloud of the base deflection

## 6.2 Design of the control device

### 6.2.1 Base design

The deformation of the slab is large due to the heavy weight of auxiliary mass. If the stiffness of the base is insufficient, its surface flatness is not good enough that will affect the AMD system operation seriously. With this consideration, we use a U-shaped base composed of two identical girders in  $10.00\text{ m} \times 0.50\text{ m} \times 1.45\text{ m}$  (long  $\times$  wide  $\times$  high). The vertical deformation under the worst condition (do not consider the dynamic effect in vertical direction) is shown in Fig. 14.

From Fig. 14 it can be seen that, the base nodes' largest and smallest vertical deformations are  $-16.95\text{ mm}$  and  $-9.09\text{ mm}$  respectively, and the largest relative deformation of base nodes is  $7.86\text{ mm}$ . The largest and smallest vertical deformations of upside surface nodes are  $-14.19\text{ mm}$  and  $-9.47\text{ mm}$  respectively, so the largest relative deformation of upside surface is  $4.72\text{ mm}$ . Ignoring the gap between supporting guide pair and base, the largest relative nodal deformation on upside surface is  $4.72\text{ mm}$ . Therefore, applying a corresponding counter-arch during the installation of base can meet the flatness requirement.

### 6.2.2 Selection of guide pair

As per to the operating conditions, heavy load rolling linear guide pair has been selected. Each guide has 5 sliding blocks and preload P0 jointed together with 4 segments with  $10\text{ m}$  long. They are in 5<sup>th</sup> grade. The specified dynamic load, static load and the moments in three directions are  $1040\text{ kN}$ ,  $1924\text{ kN}$ ,  $123176\text{ N.m}$ ,  $123176\text{ N.m}$ , and  $114438\text{ N.m}$  respectively. Each sliding block carries 25 tons load with a safety factor of 4.24. This satisfies the operating requirements.

### 6.2.3 Electrical machine

The largest driving force and input power of AMD1/AMD2 system are  $300\text{ kN}$  and  $300\text{ kW}$  respectively. The 1PL6288-3DF23-0E-A0 Siemens servo motor with  $560\text{ kW}$  power,  $280\text{ mm}$  center height and  $3055\text{ kN.m}$  torsion is used in this paper.

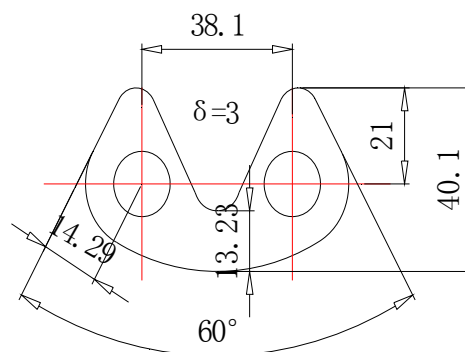


Fig. 15 size of single chain piece

### 6.2.4 Gear chain design

With consideration of the auxiliary mass, acceleration and certain safety factor as well, the chain pitch, width, and thickness of single chain piece are chosen respectively as  $38.1\text{ mm}$ ,  $254.0\text{ mm}$ , and  $3.0\text{ mm}$ . The chain is inside oriented. Each gear chain contains 85 pieces in which at least

42 pieces carry load. Single chain piece is shown in Fig. 15.

The stress of the weakest part under operating condition is

$$\begin{aligned}\sigma_{\max} &= \frac{F_{\max}}{S_{\min}} = \frac{300000 \text{ N}}{13.23 \times 3 \times 42 \times 10^{-6} \text{ m}^2} \\ &= 179.96 \text{ MPa}\end{aligned}\quad (17)$$

This value is less than the ultimate stress (235MPa) of the ordinary carbon steel Q235A, so the gear chain is safe during the normal working state.

### 6.2.5 Sprocket shaft

As per the operating parameters (largest driving force, power capacity and so on) of AMD controlling system, we choose a sprocket axis diameter equal or greater than 130 mm with 17 teeth. The single sprocket is shown in Fig. 16.

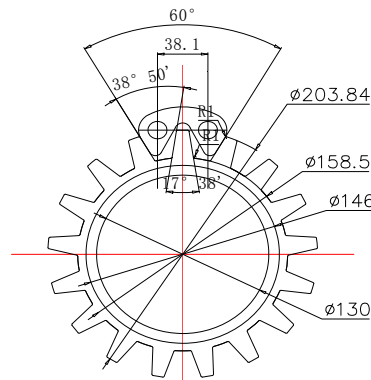


Fig. 16 chain gear and chain piece

From Fig. 16 we know the arc length of chain gear at the root end is

$$l_1 = \frac{\pi d}{2n} = \frac{3.14 \times 158.5}{2 \times 17} = 14.63 \text{ mm}\quad (18)$$

The chain width  $b=254 \text{ mm}$ , so the stress at the root end is

$$\begin{aligned}\sigma_{\max} &= \frac{F_t}{b \cdot l} = \frac{300000 \text{ N}}{14.63 \times 254 \times 10^{-6} \text{ m}^2} \\ &= 80.73 \text{ MPa}\end{aligned}\quad (19)$$

This value is less than the ultimate stress (235MPa) of the Q235A, which meets the operating requirement.

The AMD system based on the design above has the following properties:

1. The base consists of two girders with large flexural rigidity which avoids insufficient stiffness of the slab and keeps the AMD system safe.

2. Using the gear chain for transmission, the chain and the floor can deflect together thus

reducing the energy loss due to the friction between the gear and chain. This also partly solves the large energy dissipation problem of the system.

3. The hydraulic buffer installed between the auxiliary mass and supporting guide pair avoids excessive impact of urgent opening and closing of the control system, and thus guarantees the system stability and safety.

4. The gear surrounded by chains with pretension can significantly improve the sensitivity of transmission. This can also partly help solve the time delay problem of the control system.

## 7. Conclusions

This paper mainly introduced the technologies and methodologies of implementation of AMD control system on a high-rise building in Shenzhen, China. The major conclusions are as follows:

1. Considering the large quantity of DOFs of the original structure, calculation speed using the original structure model cannot satisfy the real-time online control requirements. A simplified model is used that can capture the dynamic properties of the original structure.
2. The three control algorithms developed, namely, LQR, PA, and FNN are effective in controlling the dynamic response of structure under external excitations. The control effects of PA and FNN control algorithms are almost the same, both superior compared to that of LQR control algorithm. FNN control algorithm is good at controlling the peak of structural displacement but its control effect on the structural displacement variance is not good. PA algorithm is stable and widely used, but its requirement for accuracy of calculation model is relative high. FNN requires less number of sensors being used, but its rule is associated with the stochastic wind loads.
3. Develop feedback laws to control the relative displacement (stroke) and relative velocity of the auxiliary mass simultaneously.
4. Optimal feedback gains are calculated considering the limitations on the stroke of AMD along with the reduction in dynamic response. The control algorithm proposed in this paper is flexible, and stable.
5. The proposed AMD control system in this paper successfully addressed the issues pertaining to insufficient stiffness of the building floors. The control system operates well and has a good sensitivity.

## References

- Aizawa, S. and Fukao, Y. *et al.* (1988), "An experimental study on the active mass damper", *Proceedings of the 9th World Conference on Earthquake Engineering*, Tokyo, Japan. August.
- Cao, H., Reinhorn, A.M. and Soong, T.T. (1998), "Design of an active mass damper for a tall TV tower in Nanjing, China", *Eng. Struct.*, **20**(3), 134-143.
- Chunyan, J., Huajun, L. and Qingmin, M. (2004), "Active control strategy for offshore structures accounting for AMD constraints", *High Technol. Lett.*, **10**(4), 63-68.
- Fujita, T., Kamada, T. and Masaki, N. (1992), "Fundamental study of active mass damper using multistage rubber bearing and hydraulic actuator for vibration control of tall buildings: part 1 study on control law for the active mass damper", *Trans. JSME*, **58**, 87-91.
- Ikeda, Y., Sasaki, K., Sakamoto, M. and Kobori, T. (2001), "Active mass driver system as the first application of active structural control", *Earthq. Eng. Struct. D.*, **30**(11), 1575-1595.
- Ikeda, Y. (2009), "Active and semi-active vibration control of buildings in Japan - Practical applications and

- verification”, *Struct. Control Health Monit.*, **16**(7-8), 703-723.
- Kawai, N. and Ohtsuka, M. *et al.* (1994), “A development of active response control system. Part 3: shaking table test results on variable gain control method”, *Trans. AIJ annual meeting*, 895-896. (in Japanese).
- Nishitani, A. (1998), “Application of active structural control in Japan”, *Prog. Struct. Eng. Mater.*, **1**(3), 301-307.
- Nishitani, A. and Inoue, Y. (2001), “Overview of the application of active/semiactive control to building structures in Japan”, *Earthq. Eng. Struct. D.*, **30**(11), 1565-1574.
- Nagashima, I. and Shinozaki, Y. (1997), “Variable gain feedback control technology of active mass damper and its application to hybrid structural control”, *Earthq. Eng. Struct. D.*, **26**(8), 815-838.
- Ou, J.P. (2003), *Structural vibration control-active, semi-active and intelligent control [M]*, Science Press, 56-57 and 98-125 (in Chinese).
- Soong, T.T. and Constantinou, M.C. (Eds.) (1994), *Passive and active structural vibration control in civil engineering*, CISM Lecture Notes, Springer-Verlag New York, USA.
- Suzuki, T. and Kageyama, M. *et al.* (1993), “Active vibration control system for high-rise buildings. Part 14: vibration test on variable feedback gain control”, *Trans. AIJ annual meeting*, 735-754 (in Japanese).
- Yamamoto, M., Aizawa, S., Higashino, M. and Toyama, K. (2001), “Practical applications of active mass dampers with hydraulic actuator”, *Earthq. Eng. Struct. D.*, **30**(11), 1697-1717.
- Yao, J.T.P. (1972), “Concept of structure control”, *J. Struct. Division, ASCE*, **98**(7), 1567-1574.
- Yoshida, K., Nishimura, Y. and Yonezawa, Y. (1986), “Variable gain feedback control for linear sampled-data systems with bounded control”, *Control Theory Adv. Technol.*, **2**, 313-323.